Laterally pumped GaAs/AlGaAs quantum wells as sources of broadband terahertz radiation

Reeno Reeder[a)]
Department of Electronics, Tallinn University of Technology, Ehitajate tee 5, 19086 Tallinn, Estonia

Zoran Ikonić and Paul Harrison
Institute of Microwaves and Photonics, School of Electronic and Electrical Engineering, University of Leeds, Leeds LS2 9JT, United Kingdom

Andres Udal and Enn Velmre
Department of Electronics, Tallinn University of Technology, Ehitajate tee 5, 19086 Tallinn, Estonia

(Received 28 February 2007; accepted 23 July 2007; published online 11 October 2007)

In this work we consider lateral current pumped GaAs/AlGaAs quantum wells as sources of incoherent terahertz radiation. The lateral field heats the electrons in a two-dimensional quantum layer and increases the population of higher subbands, hence also increasing the radiation power generated in spontaneous intersubband emission processes. Digitally graded quasi-parabolic and simple square quantum wells are considered, and the advantages of both types are discussed. Calculations at lattice temperatures of 77 K and 300 K, for electric fields up to 10 kV/cm, show that the optical output power of $\sim 100-200$ W/m^2 may be achieved for the 7 THz source. The main peak of the spectrum, at 7 THz, of the quasi-parabolic quantum well exceeds the black body radiation at 300 K by approximately a factor of two and by two orders of magnitude at 77 K.
 [DOI: 10.1063/1.2783779]

I. INTRODUCTION

The development of sources of terahertz radiation has become a hot topic in the last decade because of numerous prospective applications. The successful realization of terahertz quantum cascade lasers has made a huge impact on Terahertz technology. These coherent sources are able to give good levels of output power but still require low temperatures for their operation [below 164 K (Ref. 1)]. However, not all possible applications of terahertz radiation really require coherent and highly monochromatic sources. In fact, it is sometimes advantageous to have a reasonably broadband terahertz source that would preferably operate at room temperature. In this work we consider the possibility of using a relatively simple quantum well, pumped by a lateral current, as a source of incoherent terahertz radiation. This would be generated in spontaneous radiative transitions between size-quantized states and requires just electron excitation into higher states (subbands) and not any population inversion. The bandwidth of such sources is limited from below by the spontaneous transition line width, i.e., is intermediate between those obtained from lasers and from thermal sources. However, a more broadband output can be achieved by appropriately engineering the subband structure. Their emitting area can be quite large, generally limited only by the wafer size. In structures based on conventional III/V materials like GaAs/AlGaAs, the generated radiation is intrinsically polarized perpendicularly to the well layer, hence propagating in this plane, but surface-normal emission is possible by using grating-type outcouplers.

II. THEORETICAL CONSIDERATIONS

Electrons in excited subbands of a quantum well relax into lower ones mostly by scattering processes (with phonons, interface roughness, etc.) and also, though with a small efficiency, by spontaneous emission of photons. The emitted radiation is linelike, its bandwidth determined by the line broadening. Some amount of radiation is emitted even under equilibrium due to a finite population of excited subbands at any finite temperature, and the power spectrum is also linelike, because a quantum well is not a black body. Driving the system off equilibrium, e.g., by applying a lateral electric field (Fig. 1), will generally increase the population of excited subbands and hence, the generated optical power. To get a comparatively narrowband (i.e., spontaneous-emission-width-limited) emitter of this type, one can pursue one of the following two approaches. One is to use a quantum well with a number of equispaced subbands, e.g., a parabolic-like quantum well, and rely on the fact that the only strong optical transitions are those between adjacent states. In an ideal parabolic potential only these transitions

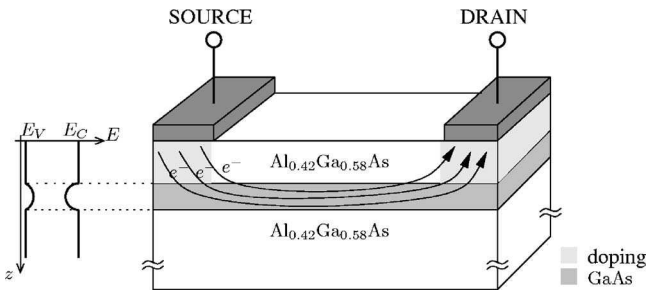

FIG. 1. Laterally pumped quantum well emitter. The doping is localized in a 2D quantum layer and in the regions under the contacts.

[a)]Electronic mail: reeno@ioc.ee

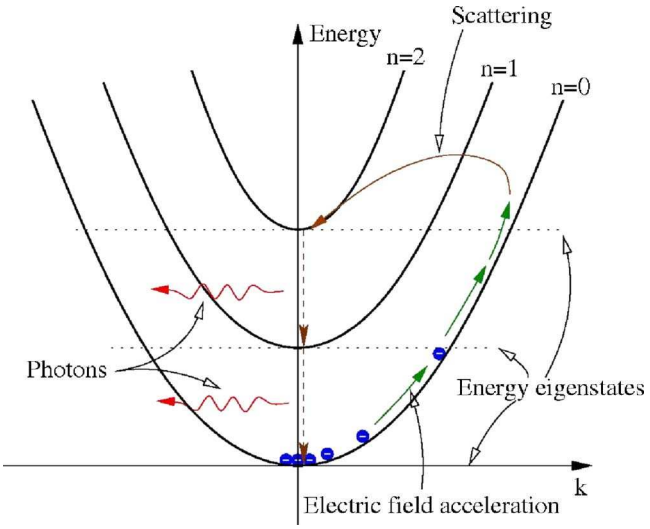

FIG. 2. (Color online) Model of subband excitation and relaxation processes.

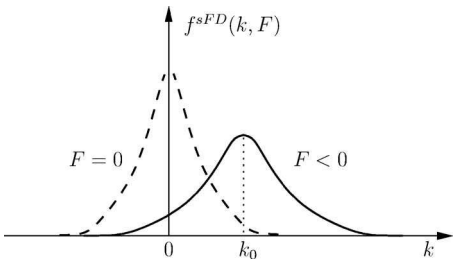

FIG. 3. Shifted distribution function. The dashed line corresponds to an equilibrium zero field case. The displayed wave vector k in the direction of the field has a shift k_0 proportional to average drift velocity of electrons. The other, perpendicular direction is not shifted, but the broadening (described by the increased electron temperature) is present in either direction.

are indeed allowed (have nonzero dipole matrix elements), but the situation is similar for many other conventional potentials. Any strong optical transition in such a system would thus contribute to the same emission profile, which would thus be independent of how strongly the system is pumped, i.e., what number of higher subbands are significantly populated. The other approach would be to use a quantum well with the lowest two states spaced by the required amount, while the third state would be much higher up and therefore unlikely to acquire a significant electron population, the situation which effectively guarantees a narrowband emission spectrum.

In either case, there is clearly a tradeoff between the pumping strength (and hence the emitted optical power) and the degree of monochromaticity of the emitted radiation, the latter being compromised by electron excitation into high subbands which cease to be equispaced (in the case of quasiparabolic wells), or into the third or higher subbands (in case of a square well). To address this question, we performed modeling of subband population dynamics in appropriate quantum wells subject to an in-plane electric field. The relevant physics is shown in Fig. 2. Electrons obtain kinetic energy from the in-plane electric field, their in-plane distribution being shifted upward along the subband. The change of the distribution modifies the electron scattering rates.[2] In particular, for sufficiently large fields the "upward" (i.e., subband-elevating) scattering rates will clearly increase, because a large fraction of electrons in a lower subband will have a large enough kinetic (and hence also the total) energy to be above a higher subband near its zone center. Electrons thus climb up the subband ladder, which results in an increased population of higher subbands compared to the equilibrium case. Electrons in higher subbands relax into lower ones not only by scattering but also by spontaneous photon emission. The generated optical power depends only on subband populations, not on the in-plane electron distribution, because optical transitions are vertical (electron wave vector conserving) and, within the parabolic in-plane dispersion model, pairs of subbands are essentially equispaced for all wave vectors. It is worth noting that considerations of hot electrons in a square well as a source of terahertz radiation have been presented in Ref. 3 but within a simple model that assumed equilibrium electron distribution throughout the system, with their temperature taken as an input parameter.

The electron distribution due to an in-plane electric field in a multisubband system may be found by solving the Boltzmann equation with all intra- and intersubband scattering processes taken into account. In this work, however, we use a simplified and much faster approach, taking the in-plane electron distribution (over the wave vectors of a subband) to be described by the shifted Maxwell–Boltzmann (MB) distribution and then explicitly handling only the intersubband scattering processes. Detailed calculations of the electron transport in bulk semiconductors show that the shifted MB distribution (see Fig. 3), with appropriate field-dependent temperature and drift velocity in the direction of the field, can be a very good approximation to the actual calculated distribution.[4] It has also been previously used, in form of a shifted Fermi–Dirac (FD) distribution, in single-subband electron-transport calculations in quantum wells.[5] In this work we apply such a model to systems with a number of size-quantized subbands and assume that each of them will have the same form of shifted-MB distribution over the in-plane wave vectors, which is then used to evaluate the distribution-averaged intersubband scattering rates, Eq. (9.153) from Ref. 6.

It should be noted that the validity of this approximation relies on having strong electron-electron intrasubband scattering, because this is the major process which brings about the electron thermalization (by which we mean that the distribution acquires the MB- or FD-like form, with its temperature generally different from that of the lattice). Under the operating conditions typical for the devices we consider ($T=77-300$ K, area doping $\sim 10^{12}$ cm^{-2}), estimates of the electron-electron intrasubband scattering time constant put it into the deep subpicosecond region.[5,7] This is much faster than any other intra- or intersubband scattering process involved in this work (slightly subpicosecond timescale, at best), and therefore using the shifted MB distribution approximation can be justified. On the other hand, it may not be necessary to explicitly include the intersubband electron-electron scattering in the rate equations. The rate of this process decreases with intersubband spacing,[6] and in view of the relatively large spacings we deal with (≈ 30 meV), we have

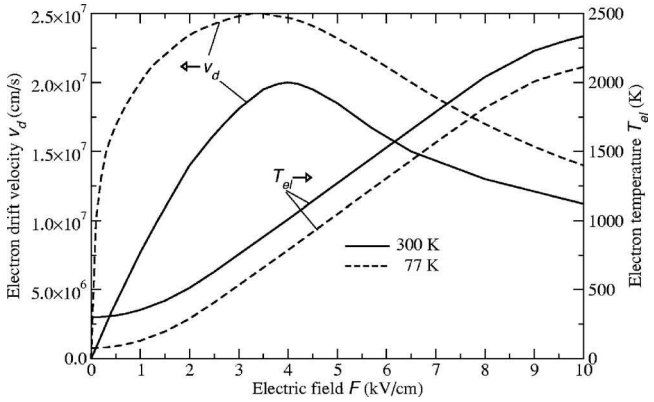

FIG. 4. Electron drift velocity and temperature dependencies on the lateral electric field used in this work, assembled from various theoretical and experimental data (Ref. 2 and 8–10).

indeed accounted only for polar LO phonon and acoustic phonon intersubband scattering, the former being the major intersubband scattering process. Since the calculation of electron-electron scattering in a multisubband system is far slower than for phonon-electron scattering, this makes large savings of computation time. At any reasonable value of the field (high enough to give technically significant effects in the system under consideration) the electron temperature is large enough that the MB and FD distributions (both shifted, in this instance) are essentially indistinguishable, and we use the latter form just for convenience.

The electron energy in the nth subband is $E_n = E_{n0} + \hbar^2 k^2 / 2m^*$, where E_{n0} is the size-quantized subband minimum energy, and the kinetic component depends on the two-dimensional (2D) in-plane wave vector k. According to the shifted-FD distribution model, the electron distribution over the in-plane k states depends not simply on their energy but is rather described as

$$f^{\mathrm{sFD}}(\mathrm{k}) = \left[1 + \exp \frac{E_{n0} + \dfrac{\hbar^2 \{[k_x - k_0(F, T_{\mathrm{latt}})]^2 + k_y^2\} - E_{F_n}}{2m^*}}{k_B T_{\mathrm{el}}(F, T_{\mathrm{latt}})} \right]^{-1}, \tag{1}$$

where $\mathbf{k} = (k_x, k_y)$ is the in-plane wave vector, E_{F_n} is the quasi-Fermi level of the nth subband, while the drift wave vector k_0 and electron temperature T_{el} both depend on the field F (here taken in the x direction) and the lattice temperature T_{latt}. For the numerical calculations the relations $k_0(F, T_{\mathrm{latt}})$ and $T_{el}(F, T_{\mathrm{latt}})$ may be obtained using data from the literature (e.g., Refs. 2 and 8–10), partly relying on the fact that the energy loss rate of the electron gas versus electron temperature dependence is almost the same for 2D and 3D systems.[11] Figure 4 shows the electron drift velocity $v_d = \hbar k_0 / m^*$ and temperature dependencies on the field, as used in this work. These were assembled using the theoretically calculated and experimental data from several sources.[2,8–10]

At equilibrium ($F=0$) the (quasi-)Fermi level is the same for all subbands, but for nonzero electric fields the subband populations n_i change, and the Fermi level for each subband is found from

$$n_i = \frac{2}{4\pi^2} \int_{k_x, k_y} f^{\mathrm{sFD}}(\mathrm{k}) dk_x dk_y. \tag{2}$$

The rate equations describing the subband population dynamics in the steady state read

$$\frac{dn_f}{dt} = \sum_{i=1}^{N} \frac{1}{\tau_{if}} n_i - n_f \sum_{i=1}^{N} \frac{1}{\tau_{fi}} = 0, \tag{3}$$

where τ_{if}^{-1} is the total averaged scattering rate from the ith to the fth subband, due to all scattering processes accounted for, and N the number of subbands included in the model. There are N such equations, making a homogeneous system. Any one of these is linearly dependent on all the others and is replaced by the particle conservation law (i.e., the global charge neutrality), $n_1 + n_2 + \ldots + n_N = N_D$, where N_D is the overall electron concentration per unit area, set by the structure doping. This makes a standard inhomogeneous linear system of equations, to be solved.

In deciding on the number of subbands to be included, one normally takes all those low-lying subbands that are expected to host a non-negligible electron population. Typical quantum well structures have a limited number of bound states (subbands), of the order of 10 or so, and including all of them present no difficulties on the computational side. However, if the actual calculation shows that even the highest bound subband becomes significantly populated at some value of the in-plane field, this is a signal that population of the above-the-barrier (continuum) subbands has begun. The model has then to be expanded to include a sufficiently large range of energies in the continuum. Since we have encountered such an operating regime, the model includes a range of continuum states, along with all the bound subbands, in the description. The continuum is described by embedding the real quantum well in a box much wider than the well width, which produces a dense spectrum of quasi-continuum states. Including any reasonable range of continuum states grossly increases the total number of states that are explicitly handled, i.e., the order N of the system [Eq. (3)], but this has to be done for sufficiently large fields.

The subband populations are thus found from the rate equations, using the distribution-averaged intersubband scattering rates, which themselves depend on the Fermi levels.[6] With this cross-dependence, it is clearly necessary to use an iterative (self-consistent) solution of the whole system, starting with arbitrary initial values, until the required precision is achieved.

With the subband populations found, the total emitted (more precisely, internally generated) optical power, due to spontaneous intersubband transitions, is calculated from

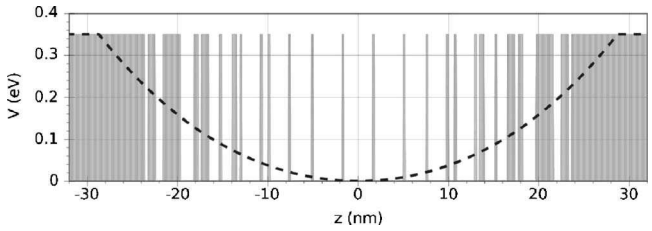

FIG. 5. Digitally graded quasiparabolic quantum well for 7 THz emission (Ref. 13). The equivalent ideal parabolic well potential is also shown. The layer widths in crystalline monolayer units, starting from the middle one (because the structure is symmetric), are as follows: **12**, 1, **11**, 1, **8**, 1, **1**, 1, **2**, 1, **7** , 1, **1**, 2, **4**, 1, **4**, 3, **1**, 2, **5**, 7, **3**, 3, **1**, bulk (GaAs - boldface, $Al_{0.42}Ga_{0.58}As$ - regular font).

$$P_{\text{total}} = \sum_{i>f}^{N} \frac{n_i}{\tau_{if}^{\text{rad}}} \hbar\omega_{if}, \tag{4}$$

where τ_{if}^{rad} and $\hbar\omega_{if}=E_i-E_f$ are the radiative lifetime and energy spacing between ith and fth subband, respectively. The radiative lifetime is given by[6]

$$\frac{1}{\tau_{if}^{\text{rad}}} = \frac{e^2\bar{n}(E_i-E_f)^3 d_{if}^2}{3\pi\varepsilon_0 c^3\hbar^4}, \tag{5}$$

where $\bar{n}$ is the refractive index, and d_{if} the optical dipole matrix element, $d_{if}=\int\Psi_f(z)z\Psi_i(z)dz$. The Lorentzian-type power spectrum is calculated from

$$P(\hbar\omega) = \sum_{i>f}^{N} \frac{n_i}{\tau_{if}^{\text{rad}}} \hbar\omega_{if} \frac{\Gamma}{\pi} \frac{1}{(\hbar\omega-\hbar\omega_{if})^2+\Gamma^2}, \tag{6}$$

where Γ is the linewidth (half width at half maximum) of the intersubband transitions, here set to 5 meV as a typical value.

III. NUMERICAL RESULTS AND DISCUSSION

In this work, the emission characteristics of the digitally graded, quasiparabolic and square wells were investigated. Continuous composition-graded wells which would provide a truncated parabolic potential, based, e.g., on $Al_xGa_{1-x}As$ alloys, are quite difficult to grow. Furthermore, a strictly parabolic composition grading does not lead to equispaced states because of the effective mass variation, though this can be corrected by modifying the composition profile.[12,13] For these reasons we have tailored a more readily realized, digitally graded quantum well, with the layer widths carefully adjusted to give 12 equispaced states to high accuracy, with the state spacing equal to approximately 29 meV, corresponding to a 7 THz radiative transition frequency.[13] The structure is shown in Fig. 5. The layer widths are integer multiples of crystalline monolayer (0.283 nm), which should minimize interface roughness.

Calculations were performed for the lattice temperatures of 300 and 77 K. Doping of 10^{12} cm^{-2}, only within the quantum well layer structure, was assumed. Using just the 12 equispaced bound states proved insufficient; hence, an additional 24 states of the quasicontinuum, covering the energy range of 0.110 eV above the barrier top, were also included in the model, because a sizeable fraction of electrons gets excited into these continuum states at larger fields. Certainly, the equispaced-states property does not apply to the continuum. The confinement box size for the quasicontinuum states was selected as 185 nm, approximately 3 times greater than the width of the QW.

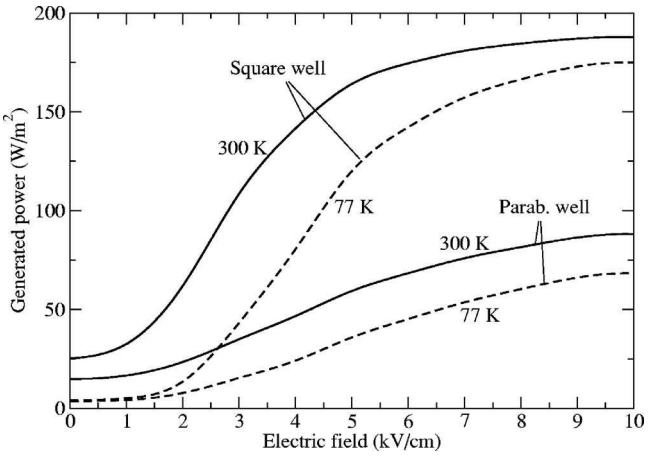

FIG. 6. Total generated optical power dependence on the lateral electric field, calculated for the digitally graded, quasiparabolic well, and for the simple square well for lattice temperatures 77 K and 300 K.

In Fig. 6 we give the total generated power dependence on the lateral electric field. This starts to increase significantly only beyond 1 kV/cm (2 kV/cm for 77 K), and enters a saturation for biases in excess of 8 kV/cm. The power range obtained, $\sim 100-200$ W/m^2, is limited by the general cubic dependence on the energy spacing [as follows from Eqs. (4) and (5), together with the fact that $d_{if}^2 \sim 1/\hbar\omega_{if}$]. The power spectrum also evolves with the field and becomes progressively less narrow, as shown in Fig. 7 for the quasiparabolic structure. For fields up to about 4–5 kV/cm the spectrum is rather "monochromatic," with a single peak around the required frequency of 7 THz, as expected from a light-emitting diode (LED) device. For higher fields, however, the side-peaks at 21 THz and 35 THz start to contribute to the output power. One can easily estimate, assuming the unity value for the surface emissivity, that the total power within the 7 THz peak at 10 kV/cm exceeds the black body radiation in the same spectral range by approximately a factor of 2, even at room temperature (300 K), and grossly exceeds it, by 2 orders of magnitude, at 77 K.

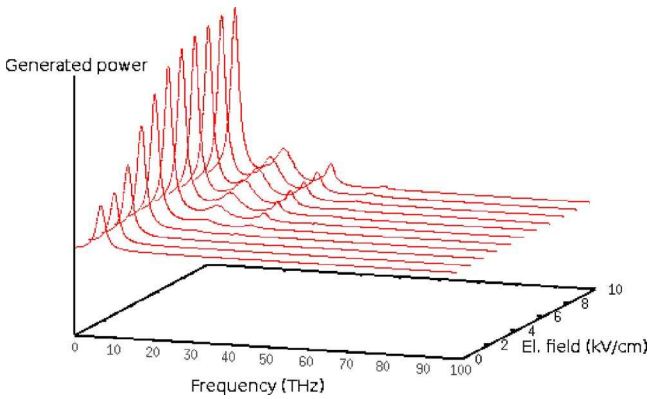

FIG. 7. (Color online) Generated power spectrum for the digitally graded quantum well. The 11 displayed spectral profiles are for electric fields of $0,1,2,\ldots 10$ kV/cm.

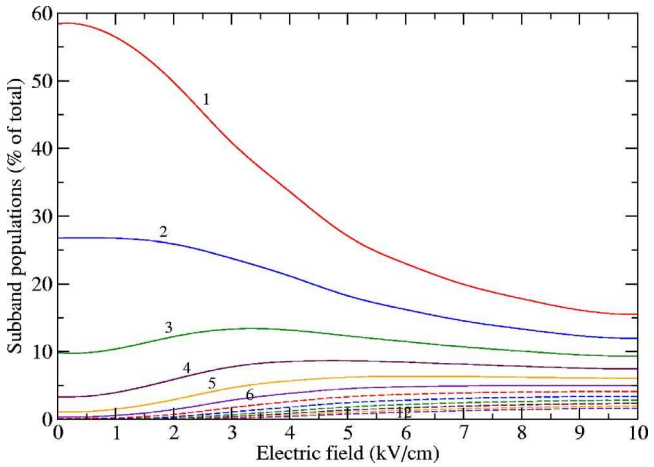

FIG. 8. (Color online) Population of the 12 equispaced bound subbands vs field dependence in the digitally graded well. The remainder of electron population belongs to the continuum.

The appearance of higher frequencies is clearly related to the increasing electron population in higher, continuum subbands, as shown in Fig. 8, which becomes quite prominent for fields above 3 kV/cm. It should be noted, however, that it may not be just electron escape to continuum which contributes to spectrum broadening. It is only the ideal parabolic potential, and not just any equispaced-states potential, which has the property that no other transitions except those between adjacent states are allowed. Indeed, starting with the parabolic potential one can generate families of asymmetric equispaced-states potentials which have quite significant transition matrix elements between more remote states.[14] However, in the digitally graded well considered here the dipole matrix elements between subbands with the quantization index changing by three are between 1 and 2 orders of magnitude smaller than those between the adjacent subbands, and others are much smaller; hence, this path for the power spectrum broadening is still of minor importance: the major part of broadening comes from the transitions from continuum states.

Another set of calculations was performed for a 20 nm wide GaAs square well embedded in a $Al_{0.3}Ga_{0.7}As$ barrier. The well width was chosen so that the energy spacing of the first two subbands is about the same as in the quasiparabolic well, i.e., approximately 30 meV. This structure has five bound subbands, at 10.1, 40.4, 90.5, 159, and 238 meV. It was embedded in a 220 nm wide outer box, and 31 quasicontinuum states were also included in the model. The calculated emission characteristics are shown in Figs. 6 and 9, and the relevant subband populations in Fig. 10. Clearly, the total power generated in this structure exceeds that of the quasiparabolic well, but the spectrum is much broader.

IV. CONCLUSION

Laterally pumped GaAs/AlGaAs quantum wells were considered as potential broadband sources of incoherent terahertz radiation, generated on spontaneous intersubband optical transitions. The in-plane field heats the electrons and hence increases the population of higher subbands, and therefore also the output power. Two types of quantum wells

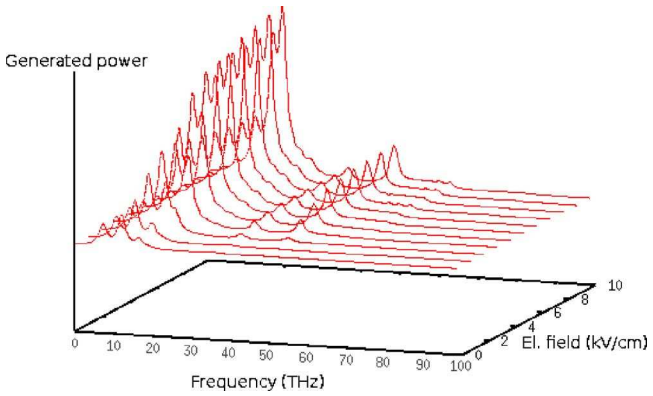

FIG. 9. (Color online) Generated power spectrum for the square well. The 11 displayed spectral profiles are for electric fields of 0,1,2,...10 kV/cm.

were considered, a digitally graded, quasiparabolic well and a simple square well, and their performance was compared. Despite the higher overall emitted power from the square well system, the emission spectrum of the quasiparabolic well is generally narrower, and up to the moderate fields remains rather monochromatic, as expected from spontaneous emission-based sources like LED devices. The total optical output power at 7 THz is limited due to the cubic dependence of the spontaneous emission on the subband energy spacing. However, the spectral power at 7 THz still exceeds, by approximately a factor of two, the ideal black body radiation at 300 K. The analysis presented predicts that this device, in contrast to quantum cascade lasers, may operate at room temperature, or even at 400 K. A higher optical output may be achieved either by increasing the electron density or by using a stack of multilayer structures. Furthermore, by appropriate modifications of the digitally graded quantum well, it appears possible to realize limited-bandwidth incoherent terahertz sources, the spectral properties of which are controllable by the built-in GaAs/AlGaAs composition distribution, and also dynamically (to an extent) by the lateral field.

ACKNOWLEDGMENTS

The authors are grateful to N. Vukmirović for helpful discussions. This work has been partly funded by Estonian

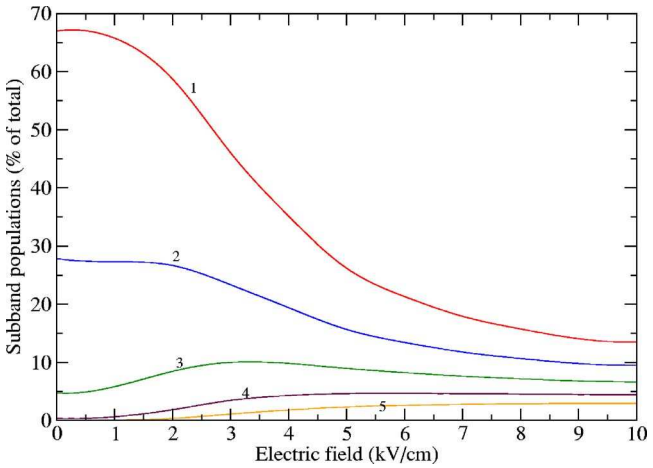

FIG. 10. (Color online) Population of the five subbands vs field dependence in the square well. The remainder of the electron population belongs to the continuum.

Science Foundation grants 5911 and 6914, the Estonian Archimedes Foundation, and the Engineering and Physical Sciences Research Consul (U.K.) THz grant EP/C002881/1.

[1]B. S. Williams, S. Kumar, Q. Hu, and J. L. Reno, Opt. Express **13**, 3331 (2005).
[2]M. Lundstrom, *Fundamentals of Carrier Transport* (Cambridge University Press, Cambridge, MA 2000).
[3]W. Xu, S. M. Stewart, D. J. Fisher, and C. Zhang, Superlattices Microstruct. **22**, 25 (1997).
[4]A. Hintz and K. Schünemann, Solid-State Electron. **35**, 165 (1992).
[5]B. A. Glavin, V. I. Pipa, V. V. Mitin, and M. A. Stroscio, Phys. Rev. B **65**, 205315 (2002).
[6]P. Harrison, *Quantum Wells, Wires and Dots* (John Wiley & Sons, Chichester, 2005).
[7]A. Mošková and M. Moško, Phys. Rev. B **61**, 3048 (2000).
[8]L. S. Tan, S. J. Chua, and V. K. Arora, Phys. Rev. B **47**, 13868 (1993).
[9]N. Fitzer, A. Kuligk, R. Redmer, M. Städele, S. M. Goodnick, and W. Schattke, Phys. Rev. B **67**, 201201 (2003).
[10]Y. M. Hsin, W. B. Tang, and H. T. Hsu, Solid-State Electron. **49**, 295 (2005).
[11]L. E. Vorobjev, S. N. Danilov, V. L. Zerova, and D. A. Firsov, Fiz. Tekh. Poluprovodn. (S.-Peterburg) **37**, 604 (2003).
[12]V. Milanović and Z. Ikonić, Phys. Rev. B **54**, 1998 (1996).
[13]R. Reeder, A. Udal, E. Velmre, and P. Harrison, *Proceedings of the 10th Biennial Baltic Electronics Conference*, Tallinn, Estonia, 2–4 Oct 2006, IEEE Cat. No. 06EX1395(2006), p. 51, Publ. Tallinn University of Technology, Tallinn, Estonia (2006).
[14]V. Milanović and Z. Ikonić, IEEE J. Quantum Electron. **32**, 1316 (1996).